Image Registration for Interventional MRI Guided Procedures: Interpolation Methods, Similarity Measurements, and Applications to the Prostate

4 authors:

Baowei Fei
The University of Texas at Dallas and UT Southwestern Medical Center
212 PUBLICATIONS **3,947** CITATIONS

SEE PROFILE

Zhenghong Lee
Case Western Reserve University
104 PUBLICATIONS **1,490** CITATIONS

SEE PROFILE

Jeffrey L Duerk
Case Western Reserve University
245 PUBLICATIONS **6,493** CITATIONS

SEE PROFILE

David L Wilson
Case Western Reserve University
355 PUBLICATIONS **5,116** CITATIONS

SEE PROFILE

Some of the authors of this publication are also working on these related projects:

Cardiac Fiber Imaging View project

Deep learning for medical image segmenation View project

Image Registration for Interventional MRI Guided Procedures: Interpolation Methods, Similarity Measurements, and Applications to the Prostate

Baowei Fei,[1] Zhenghong Lee,[2,1] Jeffery L. Duerk,[2,1] David L. Wilson[1,2]

[1] Department of Biomedical Engineering
Case Western Reserve University, Cleveland, OH 44106, USA
{BXF18, DLW} @po.cwru.edu

[2] Department of Radiology, University Hospitals of Cleveland
Cleveland, OH 44106, USA. {Lee, Duerk}@uhrad.com

Abstract. Nuclear medicine can detect and localize tumor in the prostate not reliably seen in MR. We are investigating methods to combine the advantages of SPECT with interventional MRI (iMRI) guided radiofrequency thermal ablation of the prostate. Our approach is to first register the low-resolution functional images with a high resolution MR volume. Then, by combining the high-resolution MR image with live-time iMRI acquisitions, we can, in turn, include the functional data and high-resolution anatomic information into the iMRI system for improved tumor targeting. In this study, we investigated registration methods for combining noisy, thick iMRI image slices with high-resolution MR volumes. We compared three similarity measures, i.e., normalized mutual information, mutual information, and correlation coefficient; and three interpolation methods, i.e., re-normalized sinc, tri-linear, and nearest neighbor. Registration experiments showed that transverse slice images covering the prostate work best with a registration error of ≈ 0.5 mm as compared to our volume-to-volume registration that was previously shown to be quite accurate for these image pairs.

1 Introduction

Nuclear medicine can detect and localize tumor in the prostate not reliably seen in MR.[1] We are investigating methods to combine the advantages of SPECT with interventional MRI (iMRI) guided radiofrequency (RF) thermal ablation for the treatment of the prostate cancer. Our idea is to first register the low-resolution functional images with a high resolution MRI.[2] Then by registering the high-resolution MR volume with live-time iMRI acquisitions, we can, in turn, map the functional data and high-resolution anatomic information to iMRI images to aid tumor targeting. We previously reported a method for the registration of noisy, thick iMRI image slices with high-resolution MR volumes with simulated [3] and actual iMRI images.[4] In this report, we compared three interpolation methods and three similarity measures for this application. Hundreds of registration experiments were performed with 12 pairs of MR volume images acquired from four healthy volunteers.

2 Registration Algorithms

2.1 Three Interpolation Methods

We investigated three interpolation methods, i.e., re-normalized sinc interpolation,[5] tri-linear, and nearest neighbor.

Let the original data set be I_{org}, the re-formatting data set I_{new}. The conventional sinc interpolation with a cosine Hamming window is described as below.[5,6]

$$I_{new}(x, y, z) = \sum_X \sum_Y \sum_Z I_{org}(X, Y, Z) \cdot H(x, X, R) \cdot H(y, Y, R) \cdot H(z, Z, R)$$

$$\text{where } H(a, A, R) = \frac{\sin[\pi(a - A)]}{2\pi(a - A)} \cdot \left\{ 1 + \cos[\pi(a - A) / R + 1] \right\},$$

and X, Y, Z, represent the coordinates of (I_{org}); x, y, z the coordinates of (I_{new}); A is a symbol representing $X, Y,$ or $Z,$ and a represents $x, y,$ or $z;$ and R is the kernel size. The Hamming function eliminates problems with oscillatory effects at discontinuities and guarantees that the convolution coefficients fall of to zero at the edge of the sinc kernel (i.e., at $|a|=R+1,$ where $R=5$ in this study).[5]

In our implementation, we used the re-normalized sinc interpolation method because it could make significant improvement in performance of the conventional sinc interpolation.[5] We replaced H in the above equation with

$$H_{new}(a, A, R) = H(a, A, R) \bigg/ \sum_A H(a, A, R) = H(a, A, R) \bigg/ |H(a)|.$$

2.2 Three Similarity Measurements

We used three similarity measures, normalized mutual information (NMI), mutual information (MI), and correlation coefficient (CC), in our registration. One image R is the *reference*, and the other F is *floating*. Their mutual information *MI* is given below.[7,8]

$$MI = \sum_{r,f} p_{RF}(r, f) \log \frac{p_{RF}(r, f)}{p_R(r) \cdot p_F(f)}$$

The joint probability $p_{RF}(r, f)$ and the marginal probabilities $p_R(r)$ of the reference image and $p_F(f)$ of the floating image, can be estimated from the normalized joint intensity histograms. We used the NMI version proposed by Maes.[8]

$$NMI = \frac{2MI}{H(R) + H(F)}$$

where $H(R) = -\sum_r p_R(r) \log p_R(r)$ and $H(F) = -\sum_f p_F(f) \log p_F(f).$

The correlation coefficient CC is given below.[9]

$$CC = \frac{\sum (R(r) - \overline{R})(F(f) - \overline{F})}{\sqrt{\sum (R(r) - \overline{R})^2 \sum (F(f) - \overline{F})^2}}$$

Here $\overline{R}, \overline{F}$ denote the average intensities of the reference and floating images and the summation includes all voxels within the overlap of both images.
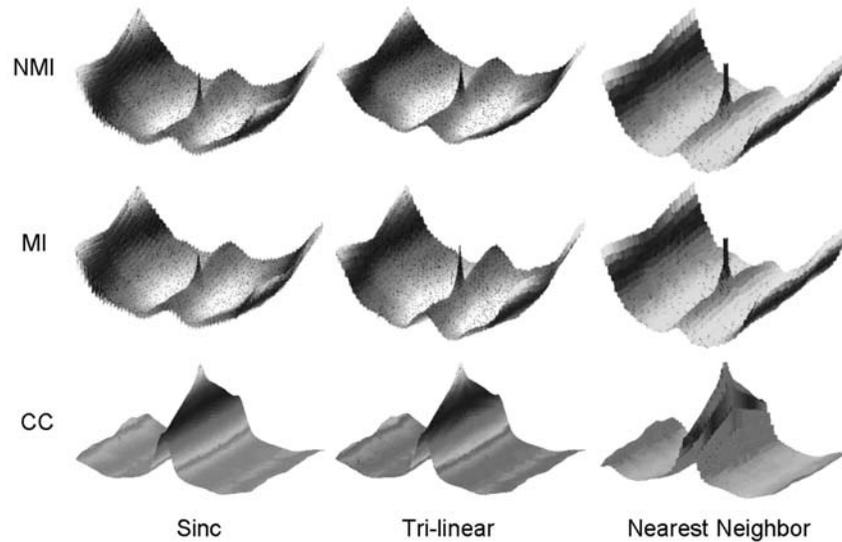

Fig. 1 Similarity surfaces are plotted as a function of translations at the 1/4 resolution in the multi-resolution registration process. Two high-resolution MRI volumes were registered, and they are down sampled by 1/4 along each linear dimension, giving a distance between voxel centers of ≈ 5.5 mm. From the optimal parameters, we computed the similarity values of the simulated iMRI and MRI images as a function of translations along the coronal (anterior-posterior) and sagittal (left-right) axis. From top to bottom, normalized mutual information (NMI), mutual information (MI), and correlation coefficient (CC) surfaces are plotted. From left to right, sinc, tri-linear, and nearest neighbor interpolations are used to obtain the floating images, respectively. The noisey NMI/MI surfaces show a false global maximum and many local maxima. CC surfaces are much smoother indicating its suitability for low resolution. Nearest neighbor has a flat peak with a width of one voxel in similarity surfaces. Images are from volunteer S2.

2.3 Comparison of Similarity Surfaces

We plot the similarity surfaces for the three similarity measures, NMI, MI, and CC, at different resolutions; and we determine their suitability for SV registration. At *1/4 resolution*, we resampled images so as to give 1/4 number of the voxels along each linear dimension. At *full resolution*, we used the full number of voxels. We plot the similarity measures as a function of translations. After two typical high-resolution MR volumes were registered,[10] values were plotted with the origin as the optimal

transformation. We calculated similarity values while moving the simulated iMRI image relative to the high-resolution MR image along coronal (anterior-posterior) and sagittal (left-right) axis. When obtaining floating images, we used the three different interpolation methods.

At 1/4 resolution (Fig. 1), CC surfaces are much smoother than NMI and MI, which are noisy and contain a false global maximum that could lead to a false answer and many local maxima.[11] From these figures, we infer that CC is better at low resolution. Comparing CC surfaces of different interpolations, sinc and tri-linear have similar surfaces, and tri-linear is better than nearest neighbor. For this application, we chose tri-linear interpolation instead of sinc because it is much faster and because it has comparable performance. Finally, we used CC and tri-linear at low resolution.

At full resolution (Fig. 2), NMI and MI surfaces are much more peaked than CC that infers good optimization accuracy, but once again there is high frequency noise in the NMI and MI curves, far from the optimum, that gives rise to local maxima that must be avoided. Comparing three interpolation methods, sinc gave the sharpest peak at the optimum; nearest neighbor interpolation gave a flat peak with a width of one voxel; and tri-linear gave a result between the other two. As stated above, tri-linear is much faster that sinc with similar performance. NMI and MI have no significant difference but NMI is a little bit robust in our implementation. We chose NMI and tri-linear at the full resolution.
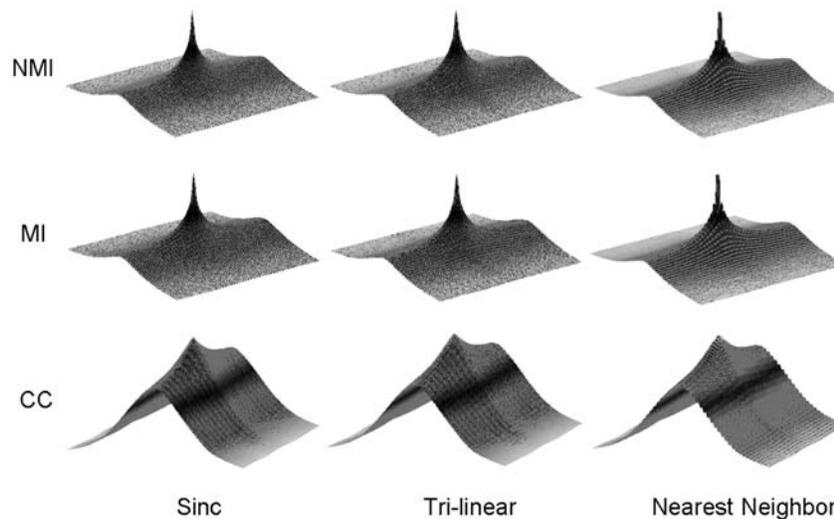

Fig. 2 Similarity functions are plotted as a function of translations at full resolution. Many details are given in the legend of Fig. 1. NMI and MI surfaces are much peaked than CC, especially with sinc and tri-linear interpolation. The voxel is isotropic with 1.4 mm on a side. Image data are the same used in Fig. 1.

2.4 Combination of Normalized Mutual Information and Correlation Coefficient

As a result of the above analyses, we created a registration algorithm for prostate MR images. We define the iMRI image slice to be the *reference* image; the matching slice from the high-resolution MRI volume is the *floating* image. We use a multi-resolution approach and perform registration from low to high resolution. We use CC at the two lower resolutions because it gives fewer local maxima and because it can be calculated faster than NMI. We use NMI at full resolution because of its peaked surface. To avoid local maxima, we include a restarting feature where registration is restarted with randomly perturbed parameters obtained from a uniform distribution about the initial transformation values at the current resolution being used. The algorithm restarts until the absolute CC is above a threshold of 0.5 as experimentally determined or the maximum number of restarts is reached.

For registration, we use a rigid body transformation (three translations and three rotations). For optimization, we use the downhill simplex method of Nelder and Mead.[12] Optimization of similarity ends either when the maximum number of calculations is reached (typically 500) or when the fractional change in the similarity function is smaller than a tolerance (typically 0.001). We use IDL (Interactive Data Language, Research System Inc., Boulder, CO.) as the programming language. We use an initial guess assuming an identity transformation, i.e., all initial translation and rotation parameters are zero, because the patient is normally oriented approximately the same way from one scan to the next. We set the maximum numbers of restarts at 10, 5, and 3, from low to high resolution, respectively.

2.5 Registration Evaluation

We used a variety of evaluation methods. We used *RegViz,* a program created in IDL in our laboratory with multiple visualization and analysis methods. First, we manually segmented prostate boundaries in image slices and copied them to corresponding slices. This enabled visual determination of the overlap of prostate boundaries over the entire volume. Second, color overlay displays were used to evaluate overlap of structures. To visualize potential differences, it was quite useful to interactively change the contribution of each image using the transparency scale. Third, we used a sector display, which divided the reference and registered images into rectangular sectors and created an output image by alternating sectors from the two input images. Even subtle shifts of edges would be clearly seen.

Our quantitative evaluation method for slice to volume registration was to compare SV and VV registration.[10] For volume pairs acquired over a short time span from a supine subject with legs flat on the table, prostates were well aligned and prostate centroid displacements were typically < 1 mm. The registration accuracy as determined from displacements of pelvic bony landmarks was 1.6 ± 0.2 mm, a value comparable to error associated with locating the landmarks.[10] To compare SV and VV registration, we defined a rectangular volume of interest (VOI) just covering the prostate and calculated voxel displacements between the two registrations. We defined the SV registration as being *successful* when the 3D displacement was less than 2.0 mm.

3 Experimental Methods

3.1 Imaging Experiments

We acquired high resolution MRI volumes from a 1.5 T Siemens MRI system (Magnetom Symphony, Siemens Medical Systems, Erlangen, Germany). An 8-element phased array body coil was used to ensure coverage of the prostate with a uniform sensitivity. We used a 3D rapid gradient echo sequence (PSIF) designed to acquire the spin-echo component of the steady state response, rather then the free induction decay. The sequence with 9.4/5.0/60 (TR/TE/flip) yielded 160 x 256 x 128 voxels over a 219 x 350 x 192-mm rectangular FOV and 1.4 x 1.4 x 1.5-mm voxels oriented to give the highest resolution for transverse slices. There was over sampling at 31% in the slice direction to reduce aliasing artifacts. The acquisition time was 4.3 min. The sequence gave excellent image contrast for the prostate and its surroundings.

We acquired high resolution MRI volumes from four volunteers S1-S4. For each volunteer, three image volumes were obtained with an imaging session. Each volume was acquired with compatible conditions. Volunteers laid supine with legs flat similar to the position in routine MR scanning. Between volume acquisitions, volunteers got off the MRI table, stretched, and walked around to ensure that they would assume a different position when they laid back on the table. The coil array was centered on the prostate. All images of a volunteer were acquired with the same MRI acquisition parameters. In total, there are 12 pairs of high-resolution MRI volumes for registration.

We used the high-resolution MRI volumes to simulate iMRI images by creating thick slices and adding noise. MR noise is described by the Rician distribution,[13] but at reasonably high signal values, the noise is accurately approximated with Gaussian white noise.[14] We added Gaussian noise to the simulated iMRI slice images. Clinically, we typically use an iMRI slice thickness of 4.0 - 6.0 mm. We averaged 3 1.4 mm thick slices to create a 4.2 mm thick slice.

Additionally, we acquired real iMRI images from volunteers S1-S3 using a clinical 0.2 T C-arm open MR scanner (Siemens Open Symphony, Erlangen, Germany). We used a two-dimensional (2D) PSIF sequence with 15.2/7.4/45 (TR/TE/FA) for image slice acquisitions. The iMRI slices were 128x128 with in-plane pixel size of 2.8x2.8 mm and with effective slice thickness of 5 mm.

3.2 Registration Experiments

We used 12 pairs of high-resolution MR volumes to perform registration experiments. For each volume pair, we extracted data from one volume to simulate thick iMRI image slices; and then we registered the simulated image slices to the other volume. We desire an iMRI slice image acquisition method that gives robust, accurate registrations and is relatively insensitive to acquisition parameters. Hence, we performed experiments to determine the dependence on slice orientation (transverse, sagittal and coronal), on slice position relative to the prostate (above, centered, and below) and on image noise from fast imaging techniques.

We also performed SV registration experiments using actual iMRI images. We registered actual iMRI image slices with high-resolution (1.5 T system) MR volumes

and visually evaluated results. For each volunteer S1-S3, there were three high-resolution MR volumes and 30 iMRI image slices giving 90 SV registration experiments, and a total of 270 experiments.
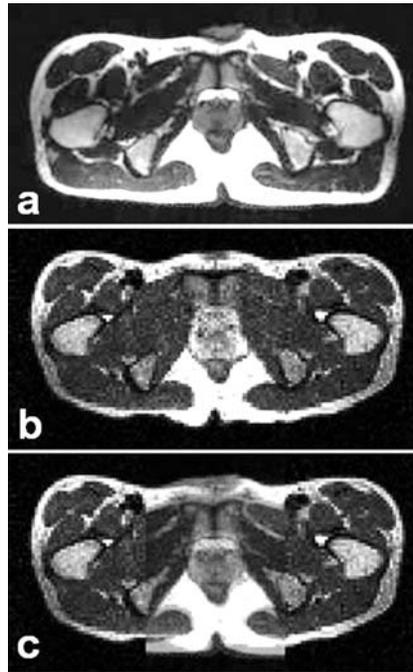

Fig. 3 Prostate images of high resolution MRI (a) and interventional MRI (b). The rectangular region at the center of image (c) is the overlay display of both images. The prostate matches well. Images are from S3.

4 Results

4.1 Simulated Images

Using simulated iMRI images, we determined SV registration results for slices near the prostate in the three standard orthogonal orientations. Comparing to VV, average registration errors were 0.4 mm, 0.5 mm, and 2.6 mm for transverse, coronal and sagittal slices covering the prostate, respectively. Transverse slices worked best because they contained many relatively rigid anatomical structures. Coronal slices worked next best. Sagittal slices gave the largest error because they contained a large portion of the deformable bladder and rectum.

The registration is insensitive to noise. Typical iMRI SNR under clinical conditions is about 25. Even when noise much exceeded this normal situation, registration results were quite good. A 100% success rate was achieved with an acceptance criterion of < 2.0 mm even when SNR was as bad as 10.

4.2 Actual iMRI Images

Registration of actual iMRI image slices with a high-resolution MR volume was successful. The contours overlap and overlay images show that the prostate matches very well. Other visual inspections also demonstrate excellent registration. Note that a single iMRI image was used to produce this registration result.

4.3 Algorithm Implementation

Computation time and registration accuracy are two main factors to consider when choosing interpolation methods. Using tri-linear interpolation, the time for an SV registration was typically about 5 sec on a Pentium IV, 1.8 GHz CPU, with 1Gbyte of memory. When the re-normalized sinc interpolation method was used, the time was ≈ 10 min, a duration not acceptable for our application. The algorithm was written in IDL and could probably be made faster in a lower level language such as C. We did not use nearest neighbor because of insufficient accuracy as deduced from its flat peak of the similarity surfaces in Figure 2. A call to the Simplex optimization typically resulted in 50 to 150 similarity evaluations before the tolerance value (0.001) was reached.

4 Discussion and Conclusion

The comparison of similarity surfaces enabled us to design a robust, fast, and accurate registration algorithm for the potential applications of iMRI-guided thermal ablation of the prostate cancer. A single iMRI image slice achieved nearly the same accuracy as obtained from volume-to-volume registration. Since live-time iMRI images are used for guidance and registered images are used for adjunctive information, the registration accuracy is very probably adequate. As compared to a typical SPECT and/or iMRI slice thickness of ≥ 3.0 mm, SV registration is quite accurate.

If one were to use functional or high-resolution MR images directly for tumor targeting within the relatively small prostate, the requirements for registration accuracy would be great. However, fused image data will not be used blindly. Rather, these visualizations will be used as a guide. Physicians will always use the live-time iMRI images for needle guidance. With proper visualization tools, physicans should be able to mentally account for any small registration errors. Moreover, the functional images might enable one to find cancer features in the iMRI images.

Finally, we conclude that it is quite feasible to include previously acquired high-resolution MRI and nuclear images into iMRI-guided treatment procedures. We are beginning to explore this application in animal experiments.

Acknowledgements

References

1. D.B.Sodee, N.Malguria, P.Faulhaber, M.I.Resnick, J.Albert, and G.Bakale, "Multicenter ProstaScint imaging findings in 2154 patients with prostate cancer," *Urology*, vol. 56, pp. 988-993, 2000.
2. Z.Lee, D.B.Sodee, J.L.Duerk, A.D.Nelson, and M.S.Berridge, "Automatic registration of SPECT-MRI in the pelvis," *Journal of Nuclear Medicine*, vol. 41, pp. 232, 2000.
3. B.W.Fei, J.L.Duerk, and D.L.Wilson, "Automatic 3D Registration for Interventional MRI-Guided Treatment of Prostate Cancer," *Computer Aided Surgery*, vol. 7, pp. 257-267, 2002.
4. B.W.Fei, J.L.Duerk, D.T.Boll, J.S.Lewin, and D.L.Wilson, "Slice to volume registration and its potential application tointerventional MRI guided radiofrequency thermal ablation of prostate cancer," *IEEE Transactions on Medical Imaging*, vol. 22, 2003.
5. N.A.Thacker, A.Jackson, D.Moriarty, and E.Vokurka, "Improved quality of re-sliced MR images using re-normalized sinc interpolation," *Journal of Magnetic Resonance Imaging*, vol. 10, pp. 582-588, 1999.
6. J.V.Hajnal, N.Saeed, E.J.SOAR, A.Oatridge, I.R.Young, and G.Bydder, "A registration and interpolation procedure for subvoxel matching of serially acquired MR images," *Journal of Computer Assisted Tomography*, vol. 19, pp. 289-296, 1995.
7. A.Collignon, F.Maes, D.Delaere, D.Vandermeulen, P.Suetens, and G.Marchal, "Automated multimodality image registration using information theory,"*Information Processing in Medical Imaging: Proc. 14th International Conference (IPMI'95)*, Computational Imaging and Vision,pp. 287-298, 1995.
8. F.Maes, A.Collignon, D.Vandermeulen, G.Marchal, and P.Suetens, "Multimodality image registration by maximization of mutual information," *IEEE Transactions on Medical Imaging*, vol. 16, pp. 187-198, 1997.
9. W.H.Press, S.A.Teukolsky, W.T.Vellerling, and B.P.Flannery. *Numerical Recipes in C: The Art of Scientific Computing, Second Edition*. New York: The Press Syndicate of the Cambridge University, 1992.
10. B.W.Fei, A.Wheaton, Z.Lee, J.L.Duerk, and D.L.Wilson, "Automatic MR volume registration and its evaluation for the pelvis and prostate," *Physics in Medicine and Biology*, vol. 47, pp. 823-838, 2002.
11. J.P.W.Pluim, J.B.A.Maintz, and M.A.Viergever, "Image registration by maximization of combined mutual information and gradient information," *IEEE Transactions on Medical Imaging*, vol. 19, pp. 809-814, 2000.
12. J.Nelder and R.A.Mead, "A simplex method for function minimization," *Computer Journal*, vol. 7, pp. 308-313, 1965.
13. A.Macovski, "Noise in MRI," *Magnetic Resonance in Medicine*, vol.36, pp. 494-497, 1996.
14. R.C.Gregg and R.D.Nowak, "Noise removal methods for high resolution MRI," *IEEE Nuclear Science Symposium*, vol. 2, pp. 1117-1121, 1997.